



# First Glycine Isomer Detected in the Interstellar Medium: Glycolamide (NH<sub>2</sub>C(O)CH<sub>2</sub>OH)

Víctor M. Rivilla<sup>1</sup>, Miguel Sanz-Novo<sup>1,2,3</sup>, Izaskun Jiménez-Serra<sup>1</sup>, Jesús Martín-Pintado<sup>1</sup>, Laura Colzi<sup>1</sup>, Shaoshan Zeng<sup>4</sup>, Andrés Megías<sup>1</sup>, Álvaro López-Gallifa<sup>1</sup>, Antonio Martínez-Henares<sup>1</sup>, Sarah Massalkhi<sup>1</sup>, Belén Tercero<sup>5</sup>, Pablo de Vicente<sup>6</sup>, Sergio Martín<sup>7,8</sup>, David San Andrés<sup>1</sup>, Miguel A. Requena-Torres<sup>9,10</sup>, and José Luis Alonso<sup>2</sup>

<sup>1</sup> Centro de Astrobiología (CAB), INTA-CSIC, Carretera de Ajalvir km 4, Torrejón de Ardoz, E-28850 Madrid, Spain; [vrivilla@cab.inta-csic.es](mailto:vrivilla@cab.inta-csic.es)

<sup>2</sup> Grupo de Espectroscopia Molecular (GEM), Edificio Quifima, Laboratorios de Espectroscopia y Bioespectroscopia, Parque Científico UVa, Universidad de Valladolid, E-47011 Valladolid, Spain

<sup>3</sup> Computational Chemistry Group, Departamento de Química Física y Química Inorgánica, Universidad de Valladolid, E-47011 Valladolid, Spain

<sup>4</sup> Star and Planet Formation Laboratory, Cluster for Pioneering Research, RIKEN, 2-1 Hirosawa, Wako, Saitama, 351-0198, Japan

<sup>5</sup> Observatorio Astronómico Nacional (OAN-IGN), Calle Alfonso XII, 3, E-28014 Madrid, Spain

<sup>6</sup> Observatorio de Yebes (OY-IGN), Cerro de la Palera SN, Yebes, Guadalajara, Spain

<sup>7</sup> European Southern Observatory, Alonso de Córdova 3107, Vitacura 763 0355, Santiago, Chile

<sup>8</sup> Joint ALMA Observatory, Alonso de Córdova 3107, Vitacura 763 0355, Santiago, Chile

<sup>9</sup> University of Maryland, College Park, MD 20742-2421, USA

<sup>10</sup> Department of Physics, Astronomy and Geosciences, Towson University, Towson, MD 21252, USA

Received 2023 June 9; revised 2023 July 3; accepted 2023 July 19; published 2023 August 18

## Abstract

We report the first detection in the interstellar medium (ISM) of a C<sub>2</sub>H<sub>5</sub>O<sub>2</sub>N isomer: *syn*-glycolamide (NH<sub>2</sub>C(O)CH<sub>2</sub>OH). The exquisite sensitivity at sub-mK levels of an ultradeep spectral survey carried out with the Yebes 40 m and IRAM 30 m telescopes toward the G+0.693–0.027 molecular cloud has allowed us to unambiguously identify multiple transitions of this species. We derived a column density of  $(7.4 \pm 0.7) \times 10^{12} \text{ cm}^{-2}$ , which implies a molecular abundance with respect to H<sub>2</sub> of  $5.5 \times 10^{-11}$ . The other C<sub>2</sub>H<sub>5</sub>O<sub>2</sub>N isomers, including the higher-energy *anti* conformer of glycolamide and two conformers of glycine, were not detected. The upper limit derived for the abundance of glycine indicates that this amino acid is surely less abundant than its isomer glycolamide in the ISM. The abundances of the C<sub>2</sub>H<sub>5</sub>O<sub>2</sub>N isomers cannot be explained in terms of thermodynamic equilibrium; thus, chemical kinetics need to be invoked. While the low abundance of glycine might not be surprising, based on the relative low abundances of acids in the ISM compared to other compounds (e.g., alcohols, aldehydes, or amines), several chemical pathways can favor the formation of its isomer glycolamide. It can be formed through radical–radical reactions on the surface of dust grains. The abundances of these radicals can be significantly boosted in an environment affected by a strong ultraviolet field induced by cosmic rays, such as that expected in G+0.693–0.027. Therefore, as shown by several recent molecular detections toward this molecular cloud, it stands out as the best target to discover new species with carbon, oxygen, and nitrogen with increasing chemical complexity.

*Unified Astronomy Thesaurus concepts:* [Astrochemistry \(75\)](#)

## 1. Introduction

Glycine (or 2-aminoacetic acid, NH<sub>2</sub>CH<sub>2</sub>COOH) is the simplest representative of amino acids, the building blocks of proteins, which play fundamental catalytic and metabolic roles in biochemistry. Given that some fundamental molecular precursors that contributed to the origin of life on Earth could have an extraterrestrial origin (e.g., Pearce et al. 2017), numerous efforts have been focused on the search for glycine in space in recent decades. Along with other amino acids, glycine has been detected in chondritic meteorites (Cronin & Pizzarello 1983; Burton et al. 2012) and, very recently, in samples provided by the JAXA Hayabusa2 mission of the asteroid Ryugu (Potiszil et al. 2023). It was also detected in the comet 67P/Churyumov–Gerasimenko by the in situ mass spectrometric analysis performed by the ESA spacecraft Rosetta (Altwegg et al. 2016). These detections put forward

the possibility of glycine being originally formed in the interstellar medium (ISM) and then incorporated into the protosolar nebula (Pizzarello et al. 2006). In the context of this latter hypothesis, glycine, along with more complex amino acids and other prebiotic chemicals, might have been delivered to early Earth through cometary and meteoritic impacts (Oró 1961; Cronin et al. 1988; Chyba 1990; Chyba & Sagan 1992; Cooper et al. 2001; Pasek 2008; Glavin & Dworkin 2009; Marty et al. 2017; Pearce et al. 2017; O’Brien et al. 2018; Rubin et al. 2019; Rivilla et al. 2020a).

Laboratory experiments have shown that glycine can be synthesized under interstellar conditions (e.g., Muñoz Caro et al. 2002; Ioppolo et al. 2021). Kuan et al. (2003) claimed the presence of glycine toward several high-mass star-forming regions, although a rigorous verification performed by Snyder et al. (2005) finally disproved these detections. Glycine has not yet been detected in the ISM despite the multiple observational efforts targeting different astronomical environments (e.g., Combes et al. 1996; Ceccarelli et al. 2000; Snyder et al. 2005; Cunningham et al. 2007; Jones et al. 2007; Jiménez-Serra et al. 2016, 2020).



Original content from this work may be used under the terms of the [Creative Commons Attribution 4.0 licence](#). Any further distribution of this work must maintain attribution to the author(s) and the title of the work, journal citation and DOI.

The nondetection of glycine might imply that it is not the most abundant member of the  $C_2H_5O_2N$  isomeric family in the ISM. Indeed, glycine is not the most thermodynamically stable isomer, and two other isomers (Sanz-Novo et al. 2019), N-methylcarbamic acid ( $CH_3NHCOOH$ ), whose microwave spectroscopy is not available, and *syn*-methyl carbamate ( $CH_3OC(O)NH_2$ ), whose search has been unfruitful so far (Demyk et al. 2004), lay below in energy. Other isomers less stable than glycine, such as glycolamide ( $NH_2C(O)CH_2OH$ ; Sanz-Novo et al. 2020; Colzi et al. 2021) and N-(Z)-hydroxyacetamide ( $CH_3C(O)NHOH$ ; Sanz-Novo et al. 2022a), remain elusive.

In this work, we have searched for all of the  $C_2H_5O_2N$  isomers for which microwave rotational spectroscopy is currently available toward the chemically rich G+0.693–0.027 molecular cloud (hereafter G+0.693), located in the Sgr B2 region of the Galactic center. Many prebiotically relevant molecules have been detected for the first time in the ISM toward this source in the last 4 yr, which makes it a very promising candidate for new discoveries (Rivilla et al. 2019, 2020b, 2021a, 2021b, 2022a, 2022b; Rodríguez-Almeida et al. 2021a, 2021b; Zeng et al. 2021; Jiménez-Serra et al. 2022). As a result of our search, we report the first detection in the ISM of a member of the  $C_2H_5O_2N$  isomeric family, the *syn* conformer of glycolamide ( $NH_2C(O)CH_2OH$ ), as well as very constraining upper limits of the abundances for the other isomers, including two conformers of glycine.

## 2. Observations

We have significantly improved the sensitivity of the spectral survey toward G+0.693 used in previous works (e.g., Zeng et al. 2020, 2021, 2023; Rivilla et al. 2021a, 2021b, 2022a, 2022b, 2022c; Rodríguez-Almeida et al. 2021a, 2021b; Colzi et al. 2022; Jiménez-Serra et al. 2022), performing new ultradeep observations with the Yebes 40 m (Guadalajara, Spain) and IRAM 30 m (Granada, Spain) telescopes. The observations, using position-switching mode, were centered at  $\alpha(\text{ICRS}) = 17^{\text{h}}47^{\text{m}}22^{\text{s}}$ ,  $\delta(\text{ICRS}) = -28^{\circ}21'27''$ , with the off position shifted by  $\Delta\alpha = -885''$  and  $\Delta\delta = 290''$ . The line intensity of the spectra was measured in units of antenna temperature ( $T_A^*$ ), since the molecular emission toward G+0.693 is extended beyond the telescope primary beams (Requena-Torres et al. 2006, 2008; Zeng et al. 2018, 2020).

The Yebes 40 m observations (project 21A014; PI: Rivilla) were carried out during multiple sessions between 2021 March and 2022 March with a total telescope scheduled time of 230 hr, of which 110 hr were on source. Part of this project, based on half of the observing runs, was presented in Rivilla et al. (2022a, 2022b). The Nanocosmos Q-band (7 mm) HEMT receiver was used, which provides ultra-broadband observations (18.5 GHz) in two linear polarizations (Tercero et al. 2021). The receiver was connected to 16 FFTs providing a channel width of 38 kHz. We observed two different spectral setups centered at 41.4 and 42.3 GHz, with a total frequency coverage of 31.07–50.42 GHz. The telescope pointing and focus were checked every 1 or 2 hr through pseudocontinuum observations. The half-power beamwidth (HPBW) of the telescope was  $\sim 35''$ – $55''$  in the observed frequency range. We performed an initial data inspection and reduction using a Python-based script<sup>11</sup> that uses the CLASS module of the GILDAS package (Megías et al. 2023). For each observing day,

we automatically fitted baselines using an iterative method that first masks the more visible lines using sigma clips and then applies rolling medians and averages, interpolating the masked regions with splines. Spectra were then combined, averaged, and imported to MADCUBA (Martín et al. 2019). The comparison of the spectra of the two frequency setups was used to identify possible spurious signals and other technical artifacts. The final spectra were smoothed to 256 kHz, which translates into velocity resolutions of 1.5–2.5  $\text{km s}^{-1}$  in the range observed, which is enough to properly characterize the typical line widths of 15–20  $\text{km s}^{-1}$  observed in the region (e.g., Requena-Torres et al. 2006; Zeng et al. 2018; Rivilla et al. 2022c). We have checked the flux density consistency between the new observations and the previous Yebes survey (e.g., Zeng et al. 2020; Rodríguez-Almeida et al. 2021a). We find that the line intensities are consistent within a 5% level. The achieved noise at this spectral resolution is 0.25–0.9 mK, depending on the spectral range.

The IRAM 30 m observations (project 123-22; PI: Jiménez-Serra) were carried out in the period of 2023 February 1–18. We used several frequency setups to cover different spectral ranges of the E0 (3 mm) and E1 (2 mm) bands of the Eight Mixer Receiver. We used the Fast Fourier Transform Spectrometer (FTS), which provides a spectral resolution of 195 kHz. We slightly shifted each setup in frequency to identify possible contamination of lines from the image band. The new spectral ranges covered were 83.2–115.41, 132.28–140.39, and 142–173.81 GHz. The HPBW is  $\sim 14''$ – $29''$ . The spectra were exported from CLASS to MADCUBA, and the reduction, including baseline subtraction, was carried out in MADCUBA. We checked the line intensities of the new observations with those of previous data (e.g., Rivilla et al. 2021b; Rodríguez-Almeida et al. 2021a), which are consistent within a 5% level. We then averaged the new data with those from the previous survey, weighting them by the noise of the spectra. The final spectra were smoothed to 615 kHz (1.0–2.2  $\text{km s}^{-1}$  in the spectral range covered). The final noise achieved is 0.5–2.5 mK at 3 mm and 1.0–1.6 mK at 2 mm. For the spectral ranges not covered by these new observations, we used the data from our previous IRAM 30 m survey (for details, refer to Rodríguez-Almeida et al. 2021a; Rivilla et al. 2022b, 2022c).

## 3. Analysis and Results

In Table 1, we list the  $C_2H_5O_2N$  isomeric family. We have searched for all of the isomers for which rotational spectroscopy is available: *syn*-methyl carbamate ( $CH_3OC(O)NH_2$ ), conformers I and II of glycine<sup>12</sup> ( $NH_2CH_2COOH$ ), conformers *syn* and *anti* of glycolamide ( $NH_2C(O)CH_2OH$ ), and the Z-conformer of N-hydroxyacetamide ( $CH_3C(O)NHOH$ ).

The exquisite sensitivity of the new observations presented here has allowed us to detect *syn*-glycolamide, which is the first  $C_2H_5O_2N$  isomer reported in the ISM. Glycolamide (or 2-hydroxyacetamide) has two conformers having  $C_s$  symmetry, with the hydroxyl ( $-OH$ ) *syn* or *anti* with respect to the carbonyl group ( $-C=O$ ). The *syn* conformer is lower in energy by  $\sim 0.9$   $\text{kcal mol}^{-1}$  (501 K; Table 1), thanks to the formation

<sup>12</sup> We note that there are up to 13 conformers of glycine (Csaszar 1992), but we include in Table 1 only the two with the lowest energy, which are the only ones with rotational spectroscopy well characterized in the laboratory.

<sup>11</sup> <https://github.com/andresmegias/gildas-class-python/>

**Table 1**  
C<sub>2</sub>H<sub>5</sub>O<sub>2</sub>N Isomeric Family

| Name                            | Formula                                | $\Delta E$<br>kcal mol <sup>-1</sup> (K) | Microwave<br>Spectroscopy | $\mu$<br>Debye     | G+0.693<br>Abundance ( $\times 10^{-10}$ ) |
|---------------------------------|--|--|---------------------------|--------------------|--|
| N-methylcarbamic acid           | CH <sub>3</sub> NHCOOH                 | 0.0 (0.0) <sup>a</sup>                   | ...                       | 2.5 <sup>a</sup>   | ...  |
| <i>syn</i> -methyl carbamate    | CH <sub>3</sub> OC(O)NH <sub>2</sub>   | 4.6 (2335) <sup>a</sup>                  | JPL 75004 <sup>c</sup>    | 2.3 <sup>a</sup>   | <2.5                                       |
| Glycine (conformer I)           | NH <sub>2</sub> CH <sub>2</sub> COOH   | 8.4 (4247) <sup>a</sup>                  | CDMS 75511 <sup>f</sup>   | 1.1 <sup>i</sup>   | <0.6                                       |
| Glycine (conformer II)          | NH <sub>2</sub> CH <sub>2</sub> COOH   | 9.2 (4650) <sup>b</sup>                  | CDMS 75512 <sup>f</sup>   | 5.5 <sup>i</sup>   | <0.019                                     |
| <i>syn</i> -glycolamide         | NH <sub>2</sub> C(O)CH <sub>2</sub> OH | 9.7 (4866) <sup>a</sup>                  | MADCUBA <sup>g</sup>      | 4.4 <sup>a</sup>   | 0.55                                       |
| <i>anti</i> -glycolamide        | NH <sub>2</sub> C(O)CH <sub>2</sub> OH | 10.6 (5367) <sup>c</sup>                 | MADCUBA <sup>g</sup>      | 2.6 <sup>g</sup>   | <0.13                                      |
| N-(hydroxymethyl)formamide      | HOCH <sub>2</sub> NHCHO                | 16.7 (8404) <sup>d</sup>                 | ...                       | 3.1 <sup>d</sup>   | ...  |
| Aminomethyl formate             | NH <sub>2</sub> CH <sub>2</sub> OCHO   | 17.7 (8907) <sup>d</sup>                 | ...                       | 1.7 <sup>d</sup>   | ...  |
| Aminoacetaldehyde               | NH <sub>2</sub> CH(OH)CHO              | 27.6 (13,889) <sup>d</sup>               | ...                       | 1.6 <sup>d</sup>   | ...  |
| 2-aminoethene-1,1-diol          | NH <sub>2</sub> CHC(OH) <sub>2</sub>   | 30.7 (15,449) <sup>d</sup>               | ...                       | 1.3 <sup>d</sup>   | ...  |
| O-acetylhydroxylamine           | CH <sub>3</sub> COONH <sub>2</sub>     | 43.5 (21,875) <sup>a</sup>               | ...                       | 1.9 <sup>a</sup>   | ...  |
| N-( <i>Z</i> )-hydroxyacetamide | CH <sub>3</sub> C(O)NHOH               | 44.7 (22,474) <sup>a</sup>               | MADCUBA <sup>h</sup>      | 3.3 <sup>a,h</sup> | <1.7                                       |
| N-hydroxyacetamidic acid        | CH <sub>3</sub> C(OH)NOH               | 45.5 (22,872) <sup>a</sup>               | ...                       | 2.5 <sup>a</sup>   | ...  |

**Notes.** Relative energies, availability of microwave spectroscopy, dipole moments, and molecular abundances derived toward G+0.693 are indicated. The “Microwave Spectroscopy” column indicates the catalog entry when available or refers to MADCUBA for catalog entries generated from published spectroscopy.

<sup>a</sup> Calculated at the CCSD(T)/aug-cc-pVTZ//MP2/aug-cc-pVTZ level by Sanz-Novo et al. (2019).

<sup>b</sup> Estimated using the B3LYP/6-311G(d,p) energy difference computed by Lattalais et al. (2011).

<sup>c</sup> Estimated using the energy difference between *syn*- and *anti*-glycolamide calculated in Maris (2004) from relative intensity and dipole moment measurements.

<sup>d</sup> Calculated at the CCSD(T)/cc-pVQZ//B3LYP/cc-pVQZ level by Lattalais et al. (2011).

<sup>e</sup> Marstokk & Mollendal (1999), Bakri et al. (2002), Ilyushin et al. (2006), and Groner et al. (2007).

<sup>f</sup> Ilyushin et al. (2005) and Lovas et al. (1995).

<sup>g</sup> Sanz-Novo et al. (2020) and Maris (2004).

<sup>h</sup> Sanz-Novo et al. (2022a).

<sup>i</sup> Lovas et al. (1995).

of a stabilizing intramolecular hydrogen bond that also hinders a possible large-amplitude motion of the –OH moiety.

For *syn*-glycolamide, we have implemented the rotational spectroscopy from the laboratory work by Sanz-Novo et al. (2020) into the Spectral Line Identification and Modeling (SLIM) tool within MADCUBA (version 9.3.10, 2023 May 4). To search for the species, we used SLIM to generate a synthetic spectrum under the assumption of local thermodynamic equilibrium (LTE) conditions. Figure 1 shows the transitions of *syn*-glycolamide detected toward G+0.693 that are unblended or only slightly blended with transitions from other species. The spectroscopic information of these transitions is presented in Table 2. To ensure that the observed spectral features are due to *syn*-glycolamide and properly evaluate possible line contamination by other molecules, we have considered the emission from the >130 molecules already identified toward G+0.693 (e.g., Requena-Torres et al. 2006, 2008; Rivilla et al. 2018, 2019, 2020b, 2021a, 2021b, 2022a, 2022b, 2022c; Zeng et al. 2018, 2021, 2023; Bizzocchi et al. 2020; Jiménez-Serra et al. 2020, 2022; Rodríguez-Almeida et al. 2021a, 2021b; Colzi et al. 2022; Alberton et al. 2023; San Andrés et al. 2023). We note that the rest of the *syn*-glycolamide transitions that fall within the spectral coverage of the survey are consistent with the observed spectra, but they are heavily blended with lines from other molecular species or too faint to be detected.

To derive the physical parameters of the emission, we used the SLIM-AUTOFIT tool of MADCUBA that provides the best nonlinear least-squares LTE fit to the data using the Levenberg–Marquardt algorithm. The parameters used in the LTE model are molecular column density ( $N$ ), excitation temperature ( $T_{\text{ex}}$ ), velocity ( $v_{\text{LSR}}$ ), and FWHM of the Gaussian line profiles. Since the molecular emission toward G+0.693 is extended and fills the telescope beams (Requena-Torres et al. 2006, 2008;

Zeng et al. 2018, 2020), no beam filling factor is used in our calculations. The fit of the *syn*-glycolamide emission was performed by using the transitions shown in Figure 1 and considering the contribution of the other identified molecules. To allow the convergence of AUTOFIT, we fixed the value of  $T_{\text{ex}}$  to 5 K, which was derived for the optically thin <sup>13</sup>C isotopologue of the simplest amide, formamide, by Zeng et al. (2023). We also fixed the FWHM to 18 km s<sup>-1</sup>, which reproduces well the profile of the most unblended lines, and we left free  $N$  and  $v_{\text{LSR}}$ . The best LTE fit is shown in Figure 1. We obtained a velocity of  $v_{\text{LSR}} = 67.0 \pm 1.0$  km s<sup>-1</sup>, which is in good agreement with the values found in G+0.693 for other molecular species, particularly amides (Zeng et al. 2023). The derived column density is  $(7.4 \pm 0.7) \times 10^{12}$  cm<sup>-2</sup>, which translates into a molecular abundance with respect to molecular hydrogen of  $5.5 \times 10^{-11}$  (Table 1), assuming  $N_{\text{H}_2} = 1.35 \times 10^{23}$  cm<sup>-2</sup> (Martín et al. 2008).

We also searched for the other C<sub>2</sub>H<sub>5</sub>O<sub>2</sub>N isomers for which spectroscopy is available (see Table 1): the higher-energy *anti* conformer of glycolamide, conformers I and II of glycine (NH<sub>2</sub>CH<sub>2</sub>COOH), *syn*-methyl carbamate (CH<sub>3</sub>OC(O)NH<sub>2</sub>), and the *Z* isomer of N-hydroxyacetamide (CH<sub>3</sub>C(O)NHOH). None of them are detected, so we computed the upper limits of their column densities using the catalog entries and spectroscopic works presented in Table 1. The detailed description of the calculations and the specific transitions used are presented in the Appendix, and the resulting upper limits are listed in Table 1.

## 4. Discussion

### 4.1. The First C<sub>2</sub>H<sub>5</sub>O<sub>2</sub>N Isomer Detected in the ISM

In spite of the many observational efforts done in the past, mainly targeting glycine, no C<sub>2</sub>H<sub>5</sub>O<sub>2</sub>N isomer was reported in

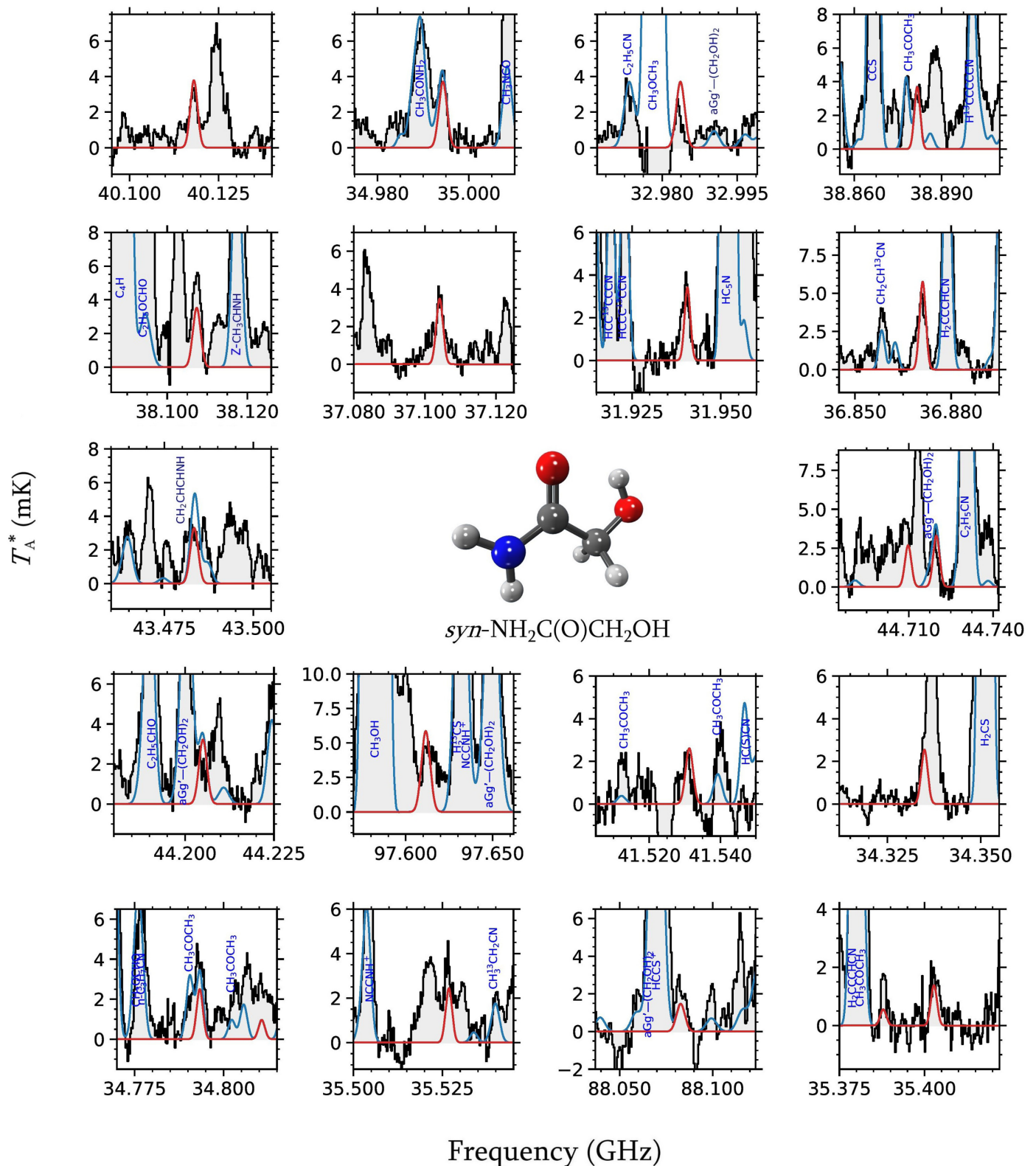


**Figure 1.** Unblended or slightly blended transitions of glycolamide detected toward the G+0.693, displayed in order of decreasing line intensity. The observed spectrum is shown as a gray histogram. The best LTE fit derived with MADCUBA for the *syn*-glycolamide emission is shown with a red curve. The blue curve represents the total modeled emission considering all of the species identified toward this molecular cloud. In the center, the molecular structure of the *syn* conformer of glycolamide is shown. Carbon atoms are in gray, oxygen atoms in red, nitrogen atoms in blue, and hydrogen atoms in white.

the ISM before the detection of glycolamide presented in this work. We discuss in this section why glycolamide is easier to detect than other isomers, particularly the long-sought glycine.

The detectability of a molecular species through rotational spectroscopy depends, obviously, on the molecular abundance but also on the strength of the dipole moment ( $\mu$ ). The larger

**Table 2**  
List of Observed Transitions of *syn*-glycolamide (*syn*-NH<sub>2</sub>C(O)CH<sub>2</sub>OH)

| Frequency<br>(GHz) | Transition<br>( $J_{K_a,K_c}$ )    | $\log I$<br>(nm <sup>2</sup> MHz) | $E_u$<br>(K) | Blending <sup>a</sup>   |
|--------------------|------------------------------------|-----------------------------------|--------------|---|
| 31.9403720         | 5 <sub>1,5</sub> -4 <sub>1,4</sub> | -5.4635                           | 4.9          | Unblended   |
| 32.9834199         | 5 <sub>0,5</sub> -4 <sub>0,4</sub> | -5.4258                           | 4.8          | Unblended   |
| 34.3346824         | 2 <sub>2,1</sub> -1 <sub>1,0</sub> | -5.7880                           | 2.3          | Partially blended with U  |
| 34.7930509         | 5 <sub>2,4</sub> -4 <sub>2,3</sub> | -5.4485                           | 6.3          | Partially blended with CH <sub>3</sub> COCH <sub>3</sub>                    |
| 34.9940974         | 5 <sub>1,5</sub> -4 <sub>0,4</sub> | -5.3948                           | 4.9          | Partially blended with <sup>13</sup> CH <sub>3</sub> CH <sub>2</sub> CN     |
| 35.4025207         | 5 <sub>3,3</sub> -4 <sub>3,2</sub> | -5.5525                           | 8.0          | Partially blended with U  |
| 35.5265875         | 2 <sub>2,0</sub> -1 <sub>1,1</sub> | -5.7941                           | 1.4          | Blended with U  |
| 36.8706638         | 6 <sub>0,6</sub> -5 <sub>1,5</sub> | -5.2658                           | 6.7          | Unblended*  |
| 36.8711421         | 5 <sub>2,3</sub> -4 <sub>2,2</sub> | -5.3969                           | 6.5          | Unblended*  |
| 37.1038814         | 5 <sub>1,4</sub> -4 <sub>1,3</sub> | -5.3359                           | 5.7          | Unblended   |
| 38.1071149         | 6 <sub>1,6</sub> -5 <sub>1,5</sub> | -5.2286                           | 6.7          | Partially blended with U  |
| 38.8813371         | 6 <sub>0,6</sub> -5 <sub>0,5</sub> | -5.2068                           | 6.7          | Unblended   |
| 40.1177882         | 6 <sub>1,6</sub> -5 <sub>0,5</sub> | -5.1784                           | 6.7          | Unblended   |
| 41.5309974         | 6 <sub>2,5</sub> -5 <sub>2,4</sub> | -5.1944                           | 8.3          | Unblended   |
| 43.4830710         | 7 <sub>0,7</sub> -6 <sub>1,6</sub> | -5.0310                           | 8.8          | Partially blended with <i>anti</i> - and <i>syn</i> -CH <sub>2</sub> CHCHNH |
| 44.2047398         | 7 <sub>1,7</sub> -6 <sub>1,6</sub> | -5.0327                           | 8.9          | Partially blended with <i>agG</i> -(CH <sub>2</sub> OH) <sub>2</sub>        |
| 44.7195221         | 7 <sub>0,7</sub> -6 <sub>0,6</sub> | -5.0209                           | 8.8          | Partially blended with <i>agG</i> -(CH <sub>2</sub> OH) <sub>2</sub>        |
| 88.0821975         | 7 <sub>3,4</sub> -6 <sub>2,5</sub> | -4.8243                           | 12.5         | Unblended   |
| 97.6105934         | 5 <sub>5,1</sub> -4 <sub>4,0</sub> | -4.4215                           | 13.3         | Unblended*  |
| 97.6111554         | 5 <sub>5,0</sub> -4 <sub>4,1</sub> | -4.4214                           | 13.3         | Unblended*  |

**Notes.** We provide the transition frequencies, quantum numbers, base 10 logarithms of the integrated intensity at 300 K ( $\log I$ ), and values of the upper levels of each transition ( $E_u$ ). The last column gives information about the line blending.

<sup>a</sup> Here “U” refers to blendings with emission from an unknown (not identified) species; transitions with an asterisk are not blended with emission from other species but (auto)blended with another transition of *syn*-glycolamide.

the dipole moment, the brighter the line intensities, and thus the easier to detect the molecule. We summarize in Table 1 the dipole moments of the different C<sub>2</sub>H<sub>5</sub>O<sub>2</sub>N isomers computed from the experimental and theoretical works cited there. The highest dipole moments are those of the higher-energy conformer of glycine (conformer II) and *syn*-glycolamide (5.5 and 4.4 D, respectively).

Besides the dipole moment, the relative energies between isomers have traditionally been used to predict whether a molecule might be present in the ISM. Lattelais et al. (2011) proposed that the isomers with higher abundances are those that are most thermodynamically stable. This empirical rule was called the minimum energy principle (MEP). However, the broad variety of new isomers detected in recent years has cast serious doubts on the applicability of the MEP. It still holds for stereoisomers (or spatial isomers),<sup>13</sup> such as the *anti* and *gauche* conformers of ethyl formate (CH<sub>3</sub>CH<sub>2</sub>(O)CHO; Tercero et al. 2013; Rivilla et al. 2017) or the *Z* and *E* isomers of cyanomethanimine (HNCHCN). Their relative isomeric ratios follow the value expected according to the thermodynamic equilibrium, which scales with  $\exp(-\Delta E/T_k)$ , where  $\Delta E$  is the energy difference between the conformers, and  $T_k$  is the kinetic temperature of the gas. García de la Concepción et al. (2021) recently demonstrated, using theoretical calculations, that this equilibrium is indeed possible in the conditions of the ISM thanks to tunneling effects that allow the isomerization.

However, it is well known that MEP fails to predict the relative abundances of many constitutional (or structural) isomers,<sup>14</sup> e.g., the C<sub>3</sub>H<sub>2</sub>O or C<sub>2</sub>H<sub>4</sub>O<sub>2</sub> isomeric families (see,

e.g., Shingledecker et al. 2019 and Mininni et al. 2020, respectively).

The analysis of the C<sub>2</sub>H<sub>5</sub>O<sub>2</sub>N isomers presented in this work confirms that the MEP does not hold for this family either. We show in Figure 2 the molecular abundances with respect to H<sub>2</sub> of the C<sub>2</sub>H<sub>5</sub>O<sub>2</sub>N isomers as a function of its relative energies, listed in Table 1. The most stable isomer with available spectroscopy is *syn*-methyl carbamate, followed by both conformers of glycine, none of them detected toward G +0.693. Glycolamide is the next isomer in terms of relative energy. The red line in Figure 2 indicates the expected molecular abundance of the C<sub>2</sub>H<sub>5</sub>O<sub>2</sub>N isomers as a function of their relative energy, in case the thermodynamic equilibrium were governing the isomeric relative abundances. We have assumed a kinetic temperature of  $T_k = 100$  K for G+0.693 (Zeng et al. 2018) and used the relative energy differences in Table 1. From thermodynamics, N-methylcarbamic acid and both glycine conformers should have much higher abundances than glycolamide, and also higher than the upper limits derived for them (blue triangles in Figure 2). Therefore, the abundances of all of the C<sub>2</sub>H<sub>5</sub>O<sub>2</sub>N isomers cannot be explained in terms of thermodynamical equilibrium; hence, they need to be described by chemical kinetics, i.e., by different formation and destruction routes for each isomer.

In the case of the most-searched isomer, glycine, its nondetection might not be surprising from an astrochemical point of view. While chemical compounds with functional groups such as -CH<sub>3</sub>, -CH<sub>2</sub>CH<sub>3</sub>, -C+N, -CH<sub>2</sub>OH, -HCO, or -NH<sub>2</sub> are common, interstellar molecules with the carboxyl group (-COOH) are remarkably scarce. So far, only the simplest representatives, formic acid (HCOOH) and acetic (CH<sub>3</sub>COOH), have been reported, and very recently, carbonic acid (HOCOOH) has also been detected (Sanz-Novo et al. 2023).

<sup>13</sup> Isomers that possess identical constitutions but differ in the three-dimensional orientations of their atoms.

<sup>14</sup> Molecular species with the same number of atoms of each element but arranged with different bonds between them.

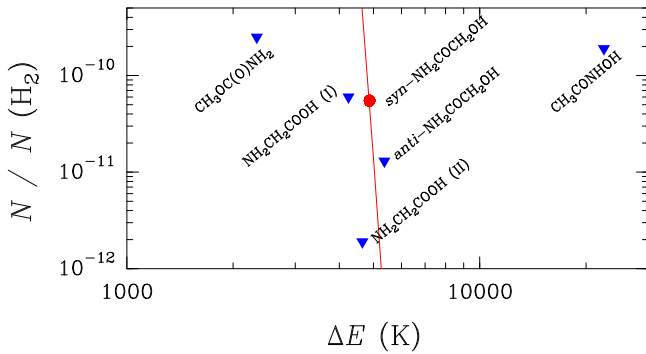


**Figure 2.** Molecular abundances with respect to  $H_2$  of  $C_2H_5O_2N$  isomers as a function of relative energy (see Table 1). The red dot corresponds to the detection of *syn*-glycolamide, while the blue triangles indicate the upper limits derived for the other isomers. The solid red line indicates the expected molecular abundance of the  $C_2H_5O_2N$  isomeric family assuming the thermodynamic population at  $T_k = 100$  K and using the abundance of *syn*-glycolamide as a reference.

Glycine ( $NH_2CH_2COOH$ ) can be seen as the amine derivative of acetic acid ( $CH_3COOH$ ), in which one H atom has been replaced by the amine group ( $NH_2$ ). Thus, we can use other H/ $NH_2$  pairs already detected toward G+0.693 to infer the expected abundance of glycine: glycolaldehyde ( $HCOCH_2OH$ ) and glycolamide ( $NH_2COCH_2OH$ ) and ethanol ( $CH_3CH_2OH$ ) and ethanolamine ( $NH_2CH_2CH_2OH$ ). The glycolaldehyde/glycolamide ratio is  $\sim 15$  (Rivilla et al. 2022a; this work), while the ethanol/ethanolamine ratio is  $\sim 40$  (Rivilla et al. 2021b; Rodríguez-Almeida et al. 2021a). If we assume these ratios for the acetic acid/glycine pair, and using the abundance of acetic acid reported by Sanz-Novo et al. (2023) of  $3.1 \times 10^{-10}$ , the abundance of glycine would be in the range of  $\sim (0.8-2) \times 10^{-11}$ . These values are a factor of 3–8 below the upper limit derived in this work for the low-energy conformer I (Table 1). As discussed in more detail in the Appendix, if both glycine conformers were in thermodynamic equilibrium, the measured upper limit derived for the high-energy conformer (II) would translate into an upper limit for the low-energy conformer of  $\sim 10^{-10}$ , very similar to that derived using conformer I itself. Hence, it is clear that the abundance of glycine toward G+0.693 is expected to be below  $10^{-10}$  and surely lower than that derived for its isomer glycolamide (see Figure 2).

Therefore, the chemistry that takes place in the ISM might be able to form glycine, but its low expected abundance makes it very challenging to detect with present-day radio telescopes at reasonable integration times. The detection of glycolamide indicates that it can be efficiently formed under interstellar conditions. In the next section, we will discuss several chemical pathways that can form glycolamide in the ISM.

#### 4.2. Formation of Glycolamide

The chemistry of G+0.693 is thought to be dominated by large-scale shocks (Martín-Pintado et al. 2001; Martín et al. 2008) produced by a cloud–cloud collision (Zeng et al. 2020). These shocks are responsible for the sputtering of dust grains, releasing many molecules formed on the grain surfaces into the gas phase (Caselli et al. 1997; Jiménez-Serra et al. 2008). Therefore, surface chemistry is expected to play a major role in G+0.693. For this reason, and because no viable gas-phase route of glycolamide has been proposed in the literature, from here on, we will consider only grain-surface reactions.

Glycolamide is the largest molecule containing an amide functional group ( $-NH-C(=O)-$ ) detected in the ISM. It is an  $\alpha$ -substitute of acetamide ( $NH_2C(O)CH_3$ ), in which one hydrogen atom of the methyl group is replaced by the hydroxyl group  $-OH$ . Based on this similarity, both amides might have similar formation routes. The chemistry of acetamide in G+0.693 has been recently discussed by Zeng et al. (2023). Chemical models (Belloche et al. 2017, 2019; Garrod et al. 2022) have suggested that the formation of acetamide involves reactions between simple radicals ( $CH_3$  and  $NH_2$ ) with larger radicals ( $NH_2CO$  and  $CH_3CO$ ) that can be synthesized on grains through H-addition and/or H-abstraction reactions of species that are abundant in the ISM and G+0.693 in particular ( $HNCO$ ,  $NH_2CHO$ ,  $H_2CCO$ , and  $CH_3CHO$ ) and/or through the combination of CO with  $NH_2$  (see the experiments of Ligterink et al. 2018) and  $CH_3$ , respectively (see Figure 3).

Analogous pathways involving radical–radical reactions, depicted in Figure 3, are promising formation routes for glycolamide. Sanz-Novo et al. (2020) proposed that it can be formed from the reaction between  $NH_2$  and the  $COCH_2OH$  radical. The latter can result from H abstraction on the formyl site of glycolaldehyde ( $HCOCH_2OH$ ), the reaction between CO with the hydroxymethyl radical ( $CH_2OH$ ), and/or the combination of the OH radical with ketene ( $H_2CCO$ ). Haupa et al. (2020) suggested that glycolamide can also be formed through the radical–radical reaction between OH and the 2-amino-2-oxoethyl radical ( $NH_2COCH_2$ ; Figure 3), which is formed by H abstraction on the methyl site of acetamide according to their experiments. A third possible route was proposed by Garrod et al. (2008): the reaction of  $NH_2CO$  (a precursor of acetamide, as mentioned above, which is formed by hydrogen abstraction from formamide) and  $CH_2OH$  (Figure 3).

All of the possible closed-shell precursors are relatively abundant toward G+0.693. Their molecular abundances with respect to  $H_2$ , in units of  $10^{-10}$ , are 266 ( $HNCO$ ; Zeng et al. 2018), 37 ( $CH_3CHO$ ; Sanz-Novo et al. 2022b), 21 ( $H_2CCO$ ; Requena-Torres et al. 2008<sup>15</sup>), 18.5 ( $NH_2CHO$ ; Zeng et al. 2023), 8.5 ( $NH_2COCH_3$ ; Zeng et al. 2023), and 6.9 ( $HCOCH_2OH$ ; Rivilla et al. 2022a), which are higher than the abundance of *syn*-glycolamide by factors of  $\sim 15$ –500. Hence, all of them are viable precursors.

Besides G+0.693, abundance upper limits of glycolamide have been derived toward the hot molecular cores Sgr B2(N2), located  $\sim 60''$  southwest of G+0.693, and G31.41+0.41 (hereafter G31), located in the Galactic disk (Sanz-Novo et al. 2020 and Colzi et al. 2021, respectively). In Figure 4, we compare the column densities (normalized to acetamide,  $NH_2C(O)CH_3$ ) derived in the three sources. We use the molecular abundances from Zeng et al. (2018), Sanz-Novo et al. (2022b), Rivilla et al. (2022a), and Zeng et al. (2023) for G+0.693; Mininni et al. (2020), Colzi et al. (2021), and private communication for G31 (V. M. Rivilla 2023, private communication); and Belloche et al. (2017) and Sanz-Novo et al. (2020) for Sgr B2(N2). The proposed precursors of glycolamide have similar molecular ratios in Sgr B2(N2) and G+0.693 within factors of 1.0–2.2, with the exception of  $NH_2CHO$ , which is an order of magnitude more abundant in Sgr B2(N2) (Belloche et al. 2017). This might imply that  $NH_2CHO$  is not the dominant precursor of  $NH_2C(O)CH_2OH$

<sup>15</sup> The molecular abundance reported by Requena-Torres et al. (2008) used an  $H_2$  column density for G+0.693 of  $4.1 \times 10^{22} \text{ cm}^{-2}$ , so we have recalculated it using the same value we have used for the other species, which is  $1.35 \times 10^{22} \text{ cm}^{-2}$  (Martín et al. 2008).

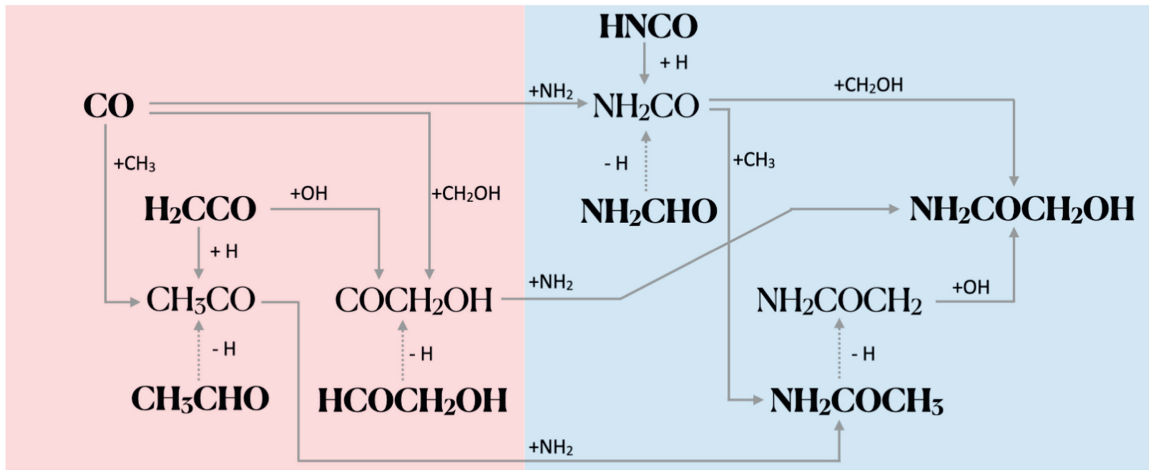


**Figure 3.** Proposed chemical network for the formation of glycolamide in the ISM. The red left panel includes oxygen-bearing species, while the blue right panel includes nitrogen- and oxygen-bearing species. Closed-shell species are labeled in bold, as opposed to radicals.

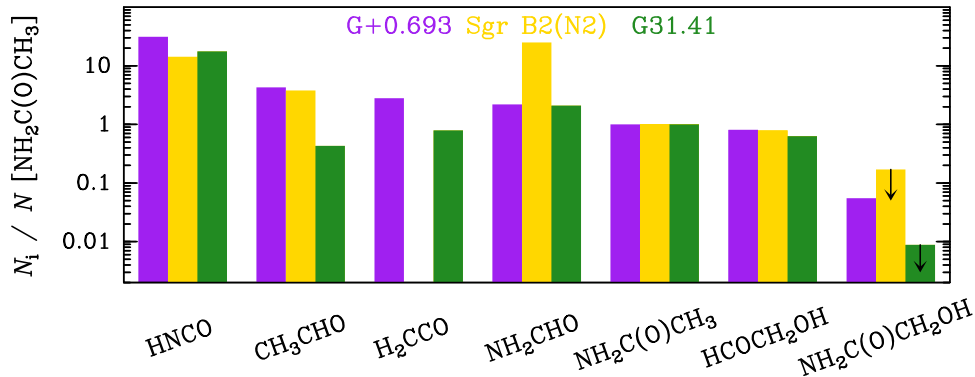


**Figure 4.** Comparison of the relative molecular abundances, compared to acetamide, of the proposed precursors of glycolamide, derived toward G+0.693 (purple) and the hot cores Sgr B2(N2) (yellow) and G31 (green). The upper limits of glycolamide are indicated with arrows.

because in that case, the formation of glycolamide would be enhanced by the same factor toward Sgr B2(N2) as compared to the other sources.

The molecular abundance ratios in G31 are very similar to those in G+0.693 within factors of  $\sim 1.0$ – $3.5$ , with the exceptions of  $\text{CH}_3\text{CHO}$  and  $\text{NH}_2\text{C}(\text{O})\text{CH}_2\text{OH}$ , which are lower by factors of  $\sim 10$  and  $>6.3$ , respectively. This might indicate that acetaldehyde and glycolamide are chemically linked. However, we note that firm conclusions cannot be drawn based on only three astronomical sources, and that the detection of glycolamide in more astronomical environments (molecular clouds, hot cores/corinos, protostellar shocks) is needed to shed light on the formation processes of glycolamide.

Since radical–radical reactions on the surface of dust grains are generally barrierless, the bottleneck of the proposed pathways is the formation of the larger radicals shown in Figure 3:  $\text{CH}_3\text{CO}$ ,  $\text{COCH}_2\text{OH}$ ,  $\text{NH}_2\text{CO}$ , and  $\text{NH}_2\text{COCH}_2$ . The detection of glycolamide toward G+0.693 suggests that the production of these radicals is more efficient than in Sgr B2(N2) and G31. These radicals can be formed from abundant closed-shell species by H abstractions and H, OH,  $\text{CH}_3$ , and  $\text{NH}_2$  additions (Figure 3). All of these mechanisms can be enhanced in the presence of a ultraviolet field induced by cosmic rays (Garrod et al. 2022). Indeed, a high cosmic-ray ionization rate (CRIR) has been derived toward G+0.693 ( $\sim 10^{-15}$ – $10^{-14}$   $\text{s}^{-1}$ ; Rivilla et al. 2022b), in good agreement with those measured in its hosting Sgr B2 region (Yusef-Zadeh et al. 2007, 2016), and across the whole Galactic

center (Goto 2013). Although Sgr B2(N2) is located close to G+0.693, the extremely high column density of  $\text{H}_2$  in the hot core ( $\sim 10^2$ , Sánchez-Monge et al. 2017, much higher than that of G+0.693 of  $\sim 10^{23}$   $\text{cm}^{-2}$ ) is expected to drastically attenuate the CRIR (Padovani et al. 2013). Similarly, G31 is exposed to a much lower cosmic-ray flux because it is located in the Galactic disk, where the CRIR is 2–3 orders of magnitude lower than in the Galactic center, which is further attenuated due to the high  $\text{H}_2$  column density of the molecular core ( $\sim 10^{25}$   $\text{cm}^{-2}$ ; Mininni et al. 2020). In summary, the formation of complex molecules such as  $\text{NH}_2\text{COCH}_2\text{OH}$  on the grain surfaces through filling reactions is expected to be boosted in the presence of high CRIR, like that present in G+0.693.

## 5. Summary and Conclusions

We have searched for members of the isomeric family of glycine ( $\text{C}_2\text{H}_5\text{O}_2\text{N}$ ) toward the G+0.693–0.027 molecular cloud located in the Galactic center using new ultradeep observations carried out with the Yebes 40 m and IRAM 30 m telescopes with improved sensitivity at sub-mK levels. We present the first detection in the ISM of a  $\text{C}_2\text{H}_5\text{O}_2\text{N}$  isomer: the *syn* conformer of glycolamide ( $\text{NH}_2\text{C}(\text{O})\text{CH}_2\text{OH}$ ). We have derived a column density of  $(7.4 \pm 0.7) \times 10^{12}$   $\text{cm}^{-2}$ , which translates into a molecular abundance with respect to molecular hydrogen of  $5.5 \times 10^{-10}$ . We also report upper limits of the molecular abundances of five other isomers: the *anti* conformer

of glycolamide, conformers I and II of glycine ( $\text{NH}_2\text{CH}_2\text{COOH}$ ), *syn*-methyl carbamate ( $\text{CH}_3\text{OC}(\text{O})\text{NH}_2$ ), and *N*-(*Z*)-hydroxyacetamide ( $\text{CH}_3\text{C}(\text{O})\text{NHOH}$ ). The upper limit for the low-energy conformer of glycine is  $<0.6 \times 10^{-10}$ , which indicates that it is less abundant than *syn*-glycolamide. The relative abundances of the  $\text{C}_2\text{H}_5\text{O}_2\text{N}$  isomers cannot be described in terms of thermodynamics; thus, they are due to different chemical pathways in the ISM that favor the formation of glycolamide over other isomers. We discuss different routes to produce glycolamide on the surface of dust grains based on reactions between simple radicals ( $\text{OH}$ ,  $\text{NH}_2$ ,  $\text{CH}_3$ , and  $\text{CH}_2\text{OH}$ ) and larger radicals generated from abundant precursors already detected in the cloud ( $\text{CO}$ ,  $\text{HNCO}$ ,  $\text{CH}_3\text{CHO}$ ,  $\text{NH}_2\text{CHO}$ ,  $\text{H}_2\text{CCO}$ ,  $\text{HCOCH}_2\text{OH}$ , or  $\text{NH}_2\text{COCH}_3$ ) after H, OH, and  $\text{NH}_2$  additions and/or H abstractions. The formation of these radicals is expected to be enhanced in the presence of the intense cosmic-ray secondary ultraviolet field likely present in G+0.693, providing a natural explanation for the detection of glycolamide and opening the window for the detection of equally or even more complex species.

### Acknowledgments

We acknowledge the two anonymous reviewers for their careful reading of the manuscript and useful comments. We are grateful to the IRAM 30 m and Yebes 40 m telescope staff for their help during the different observing runs. The 40 m radio telescope at Yebes Observatory is operated by the Spanish Geographic Institute (IGN; Ministerio de Transportes, Movilidad y Agenda Urbana). IRAM is supported by INSU/CNRS (France), MPG (Germany), and IGN (Spain). V.M.R. acknowledges support from project RYC2020-029387-I funded by MCIN/AEI/10.13039/501100011033. M.S.N. is thankful for the financial funding from the European Union—NextGenerationEU, Ministerio de Universidades, and the University of Valladolid under a postdoctoral Margarita Salas Grant, as well as financial support from the Spanish Ministerio de Ciencia e Innovación (PID2020-117742GB-I00). I.J.-S., J.M.-P., L.C., A.M., and A.M.-H. acknowledge funding from grant Nos.

PID2019-105552RB-C41 and MDM-2017-0737 (Unidad de Excelencia María de Maeztu-Centro de Astrobiología, INTA-CSIC) by the Spanish Ministry of Science and Innovation/State Agency of Research MCIN/AEI/10.13039/501100011033 and “ERDF A way of making Europe.” D.S.A. acknowledges the funds provided by the Consejo Superior de Investigaciones Científicas (CSIC) and the Centro de Astrobiología (CAB) through project 20225AT015 (Proyectos intramurales especiales del CSIC). P.d.V. and B.T. are thankful for the support from the Spanish Ministerio de Ciencia e Innovación (MICIU) through project PID2019-107115GB-C21. B.T. also thanks the Spanish MICIU for funding support from grant PID2019-106235GB-I00. J.L.A. acknowledges the funding from the Spanish Ministerio de Ciencia e Innovación (PID2019-111396GB-I00) and European Research Council ERC-2013-SyG, grant agreement No. 610256 NANOCOSMOS.

*Software:* Madrid Data Cube Analysis (MADCUBA) on ImageJ is a software developed at the Center of Astrobiology (CAB) in Madrid, <https://cab.inta-csic.es/madcuba/> (Martín et al. 2019); GILDAS, <https://www.iram.fr/IRAMFR/GILDAS>.

### Appendix

#### Upper Limits of Nondetected $\text{C}_2\text{H}_5\text{O}_2\text{N}$ Isomers

We have also searched for other  $\text{C}_2\text{H}_5\text{O}_2\text{N}$  isomers for which rotational spectroscopy is available, which are not detected. We have thus derived  $3\sigma$  upper limits for their molecular abundances, where  $\sigma$  is the rms noise of the spectra. We used the brightest transitions predicted by the LTE model that appear completely unblended, which are listed in Table A1. For consistency, we used the same  $T_{\text{ex}}$ ,  $v_{\text{LSR}}$ , and FWHM values of the detected *syn* conformer of glycolamide.

For the high-energy *anti* conformer of glycolamide, we imported into SLIM the spectroscopic parameters reported in Table 2 of Sanz-Novo et al. (2020), which include the experimental measurements and dipole moment calculations from Maris (2004). We used the hyperfine transitions  $5_{0,5}-4_{0,4}$  (at 32.9205744 and 32.9208273 GHz), shown in Figure A1.

**Table A1**  
Transitions Used to Compute the Molecular Abundance Upper Limits for the  $\text{C}_2\text{H}_5\text{O}_2\text{N}$  Isomers Not Detected toward G+0.693

| Species                      | Formula   | Transition                             | Frequency (GHz) | $\log I$ ( $\text{nm}^2$ MHz) | $E_u$ (K) |
|------------------------------|---|--|-----------------|-------------------------------|-----------|
| <i>anti</i> -glycolamide     | $\text{NH}_2\text{C}(\text{O})\text{CH}_2\text{OH}$ | $5_{0,5,6}-4_{0,4,5}$ <sup>a</sup>     | 32.9205744      | −5.9032                       | 4.8       |
|                              |   | $5_{0,5,5}-4_{0,4,4}$                  | 32.9208273      | −5.9935                       | 4.8       |
| Glycine (conformer I)        | $\text{NH}_2\text{CH}_2\text{COOH}$                 | $5_{1,5}-4_{1,4}$ <sup>b</sup>         | 31.1583057      | −6.5064                       | 4.8       |
|                              |   | $5_{0,4}-4_{0,4}$                      | 32.2028617      | −6.4669                       | 4.7       |
| Glycine (conformer II)       | $\text{NH}_2\text{CH}_2\text{COOH}$                 | $6_{2,5}-5_{2,4}$ <sup>b</sup>         | 41.9020415      | −4.6541                       | 8.3       |
| <i>syn</i> -methyl carbamate | $\text{CH}_3\text{OC}(\text{O})\text{NH}_2$         | $2_{2,0,2}-1_{1,1,1}$ A <sup>c,d</sup> | 36.7150325      | −7.1378                       | 2.4       |
|                              |   | $2_{2,0,2}-1_{1,1,2}$ A                | 36.7156362      | −7.6149                       | 2.4       |
|                              |   | $2_{2,0,1}-1_{1,1,1}$ A                | 36.7164348      | −7.6150                       | 2.4       |
|                              |   | $2_{2,0,3}-1_{1,1,2}$ A                | 36.7165377      | −6.8668                       | 2.4       |
|                              |   | $2_{2,0,1}-1_{1,1,0}$ A                | 36.7179444      | −7.4900                       | 2.4       |
|                              |   | $6_{1,6,7}-5_{0,5,6}$ A <sup>d</sup>   | 40.8305064      | −6.6448                       | 6.9       |

**Notes.** We provide the quantum numbers, transition frequencies, base 10 logarithms of the integrated intensity at 300 K ( $\log I$ ), and values of the upper levels for each transition ( $E_u$ ).

<sup>a</sup> For *anti*-glycolamide and *N*-(*Z*)-hydroxyacetamide, the Hamiltonian was set up in the coupled basis set  $I + J = F$ , so the energy levels involved in each transition are labeled with the quantum numbers  $J$ ,  $K_a$ ,  $K_c$ , and  $F$ .

<sup>b</sup> For the glycine conformers, the quantum numbers are  $J$ ,  $K_a$ , and  $K_c$ .

<sup>c</sup> For *syn*-methyl carbamate, an internal rotor Hamiltonian was used, and the hyperfine structure was also considered.

<sup>d</sup> The A label refers to the A-symmetry states of *syn*-methyl carbamate and *N*-(*Z*)-hydroxyacetamide, which is due in both cases to the presence of a methyl internal rotation motion.

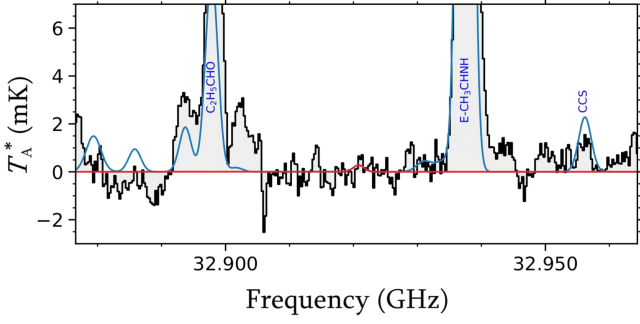


**Figure A1.** Transition of *anti*-glycolamide (*anti*-NH<sub>2</sub>C(O)CH<sub>2</sub>OH) used to derive its column density upper limit. The observed spectrum is shown as a gray histogram, and the LTE synthetic model using the derived upper limit is shown with a red curve.

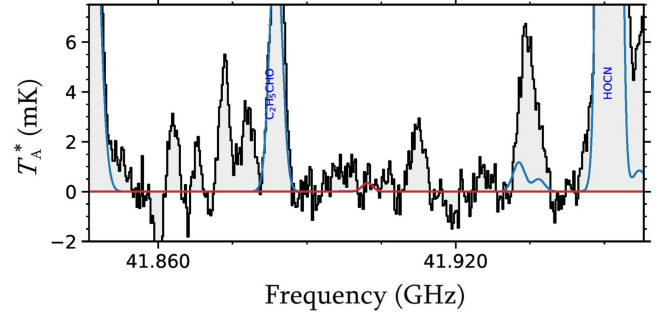


**Figure A3.** Transitions of conformer II of glycine (NH<sub>2</sub>CH<sub>2</sub>COOH) used to derive its column density upper limit. The observed spectrum is shown as a gray histogram, and the LTE synthetic model using the derived upper limit is shown with a red curve.

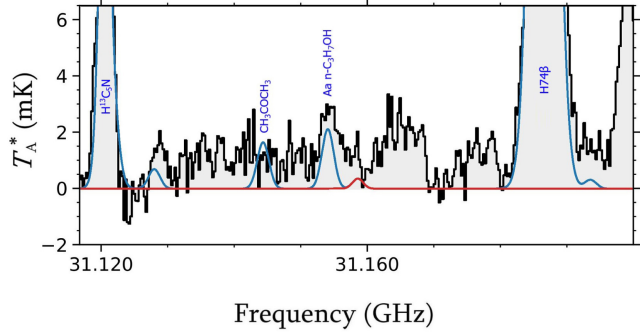
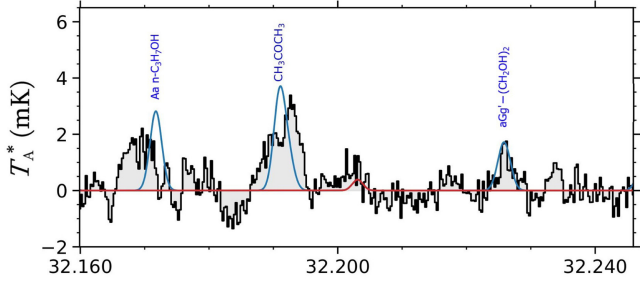


**Figure A2.** Transitions of conformer I of glycine (NH<sub>2</sub>CH<sub>2</sub>COOH) used to derive its column density upper limit. The observed spectrum is shown as a gray histogram, and the LTE synthetic model using the derived upper limit is shown with a red curve.

We obtained  $N < 1.7 \times 10^{12} \text{ cm}^{-2}$ , which translates into a molecular abundance compared to H<sub>2</sub> of  $0.13 \times 10^{-10}$  (Table 1). The derived *syn/anti* ratio is  $>4.4$ , which is consistent with the one predicted if both conformers follow thermodynamic equilibrium, as observed for other species in the ISM (e.g., Rivilla et al. 2017, 2019; García de la Concepción et al. 2021). Using their relative energy difference ( $\Delta E = 501$  K; see Table 1) and a kinetic temperature of  $T_k = 100$  K for G+0.693 (Zeng et al. 2018), their expected relative ratio would be *syn/anti*  $> 150$ , which indicates that the detection of the *anti* conformer would be challenging.

For conformers I and II of glycine (NH<sub>2</sub>CH<sub>2</sub>COOH), we used Cologne Database for Molecular Spectroscopy (CDMS; Endres et al. 2016) entries 75511 and 75512, respectively. For conformer I, we used the transitions  $5_{1,5}-4_{1,4}$  and  $5_{0,4}-4_{0,4}$  at 31.1583057 and 32.2028617 GHz, respectively. For conformer II, we used the transition  $6_{2,5}-5_{2,4}$  at 41.9020415 GHz. These transitions are shown in Figures A2 and A3, respectively. We obtained  $N < 8.1 \times 10^{12}$  and  $2.5 \times 10^{11} \text{ cm}^{-2}$  for glycine

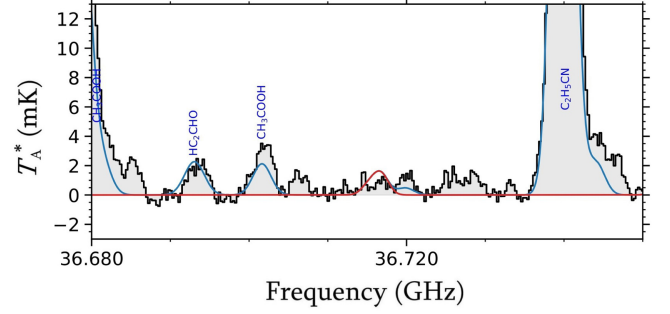


**Figure A4.** Transition of *syn*-methyl carbamate (CH<sub>3</sub>OC(O)NH<sub>2</sub>) used to derive its column density upper limit. The observed spectrum is shown as a gray histogram, and the LTE synthetic model using the derived upper limit is shown with a red curve.

conformers I and II, respectively. The upper limits of the molecular abundances are  $<0.6 \times 10^{-10}$  and  $<0.019 \times 10^{-10}$ , respectively (Table 1). The upper limit derived for the high-energy conformer II is much lower because its dipole moment is larger by a factor of 5 (see Table 1). If both conformers were in thermodynamic equilibrium, from the upper limit of conformer II, we could predict the expected column density of conformer I. Using their relative energy ( $\Delta E = 403$  K; see Table 1) and assuming  $T_k = 100$  K, the ratio between the conformers would be  $\sim 56$ . Using this ratio, the upper limit of the low-energy conformer I would be  $\sim 1 \times 10^{-10}$ , very similar to that derived directly using conformer I transitions (Table 1).

*Syn*-methyl carbamate (CH<sub>3</sub>OC(O)NH<sub>2</sub>) is the lowest-energy C<sub>2</sub>H<sub>5</sub>O<sub>2</sub>N isomer for which rotational spectroscopy is available (Table 1). To compute its abundance upper limit, we used Jet Propulsion Laboratory (JPL) catalog (Pickett et al. 1998) entry 75004. We used the five hyperfine components of the  $2_{2,0}-1_{1,1}$  transition at  $\sim 36.72$  GHz (Figure A4), which provides  $N < 3.3 \times 10^{13} \text{ cm}^{-2}$ , i.e., a molecular abundance of  $<2.5 \times 10^{-10}$  (Table 1).

Similar to glycolamide, N-hydroxyacetamide (or acetohydroxamic acid, CH<sub>3</sub>CONHOH) is a derivative of acetamide, in which a H atom of the amine group is replaced by the hydroxyl group. Its lower-energy conformer is the Z-conformer, whose spectroscopy was presented in Sanz-Novo et al. (2022a). Although an upper limit toward G+0.693 was also reported in this work, we recalculate it here using the new deeper observations and the same values of  $T_{\text{ex}}$ ,  $v_{\text{LSR}}$ , and FWHM used for the other C<sub>2</sub>H<sub>5</sub>O<sub>2</sub>N isomers. To derive the upper limit to the column density, we have used the  $6_{1,6}-5_{0,5}$  transition at

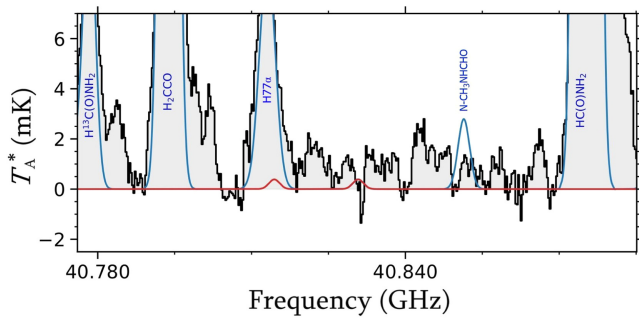


**Figure A5.** Transition of N-(Z)-hydroxyacetamide ( $\text{CH}_3\text{C}(\text{O})\text{NHOH}$ ) used to derive its column density upper limit. The observed spectrum is shown as a gray histogram, and the LTE synthetic model using the derived upper limit is shown with a red curve.

40.8305064 GHz (Figure A5), which was also used by Sanz-Novo et al. (2022a). We obtained  $N < 2.3 \times 10^{13} \text{ cm}^{-2}$ , i.e., a molecular abundance of  $< 1.7 \times 10^{-10}$  (Table 1), slightly lower than that reported by Sanz-Novo et al. (2022a) using previous observations and assuming  $T_{\text{ex}} = 8 \text{ K}$  and  $\text{FWHM} = 20 \text{ km s}^{-1}$ .

### ORCID iDs

Víctor M. Rivilla <https://orcid.org/0000-0002-2887-5859>  
 Miguel Sanz-Novo <https://orcid.org/0000-0001-9629-0257>  
 Izaskun Jiménez-Serra <https://orcid.org/0000-0003-4493-8714>  
 Jesús Martín-Pintado <https://orcid.org/0000-0003-4561-3508>  
 Laura Colzi <https://orcid.org/0000-0001-8064-6394>  
 Shaoshan Zeng <https://orcid.org/0000-0003-3721-374X>  
 Andrés Megías <https://orcid.org/0000-0002-6389-7172>  
 Álvaro López-Gallifa <https://orcid.org/0000-0001-6049-9366>  
 Antonio Martínez-Henares <https://orcid.org/0000-0001-5191-2075>  
 Sarah Massalkhi <https://orcid.org/0000-0002-7387-9787>  
 Belén Tercero <https://orcid.org/0000-0002-4782-5259>  
 Pablo de Vicente <https://orcid.org/0000-0002-5902-5005>  
 Sergio Martín <https://orcid.org/0000-0001-9281-2919>  
 David San Andrés <https://orcid.org/0000-0001-7535-4397>  
 Miguel A. Requena-Torres <https://orcid.org/0009-0009-5346-7329>  
 José Luis Alonso <https://orcid.org/0000-0002-3146-8250>

### References

- Alberton, D., Bizzocchi, L., Jiang, N., et al. 2023, *A&A*, 669, A93  
 Altwegg, K., Balsiger, H., Bar-Nun, A., et al. 2016, *SciA*, 2, e1600285  
 Bakri, B., Demaison, J., Kleiner, I., et al. 2002, *JMoSp*, 215, 312  
 Belloche, A., Garrod, R. T., Müller, H. S. P., et al. 2019, *A&A*, 628, A10  
 Belloche, A., Meshcheryakov, A. A., Garrod, R. T., et al. 2017, *A&A*, 601, A49  
 Bizzocchi, L., Prudenzano, D., Rivilla, V. M., et al. 2020, *A&A*, 640, A98  
 Burton, A. S., Stern, J. C., Elsila, J. E., Glavin, D. P., & Dworkin, J. P. 2012, *Chem. Soc. Rev.*, 41, 5459  
 Caselli, P., Hartquist, T. W., & Havnes, O. 1997, *A&A*, 322, 296  
 Ceccarelli, C., Castets, A., Caux, E., et al. 2000, *A&A*, 355, 1129  
 Chyba, C., & Sagan, C. 1992, *Natur*, 355, 125  
 Chyba, C. F. 1990, *Natur*, 343, 129  
 Colzi, L., Martín-Pintado, J., Rivilla, V. M., et al. 2022, *ApJL*, 926, L22  
 Colzi, L., Rivilla, V. M., Beltrán, M. T., et al. 2021, *A&A*, 653, A129  
 Combes, F., Q-Rieu, N., & Wlodarczak, G. 1996, *A&A*, 308, 618  
 Cooper, G., Kimmich, N., Belisle, W., et al. 2001, *Natur*, 414, 879  
 Cronin, J., & Pizzarello, S. 1983, *AdSpR*, 3, 5  
 Cronin, J. R., Pizzarello, S., & Cruikshank, D. P. 1988, in *Meteorites and the Early Solar System*, ed. J. F. Kerridge & M. S. Matthews (Tucson, AZ: Univ. of Arizona Press), 819  
 Csaszar, A. G. 1992, *JChS*, 114, 9568  
 Cunningham, M. R., Jones, P. A., Godfrey, P. D., et al. 2007, *MNRAS*, 376, 1201  
 Demyk, K., Wlodarczak, G., & Dartois, E. 2004, in *SF2A-2004: Semaine de l'Astrophysique Française*, ed. F. Combes et al. (Paris: EDP-Sciences), 493  
 Endres, C. P., Schlemmer, S., Schilke, P., Stutzki, J., & Müller, H. S. P. 2016, *JMoSp*, 327, 95  
 García de la Concepción, J., Jiménez-Serra, I., Carlos Corchado, J., Rivilla, V. M., & Martín-Pintado, J. 2021, *ApJL*, 912, L6  
 Garrod, R. T., Jin, M., Matis, K. A., et al. 2022, *ApJS*, 259, 1  
 Garrod, R. T., Widicus Weaver, S. L., & Herbst, E. 2008, *ApJ*, 682, 283  
 Glavin, D. P., & Dworkin, J. P. 2009, *PNAS*, 106, 5487  
 Goto, M. 2013, in *Proc. IAU, The cosmic ray ionization rate in the central parsec of the Galaxy*, 9, ed. L.-O. Sjouwerman, C.-C. Lang, & J. Ott (Cambridge: Cambridge Univ. Press), 429  
 Groner, P., Winniewisser, M., Medvedev, I. R., et al. 2007, *ApJS*, 169, 28  
 Haupa, K. A., Ong, W.-S., & Lee, Y.-P. 2020, *PCCP*, 22, 6192  
 Ilyushin, V., Alekseev, E., Demaison, J., & Kleiner, I. 2006, *JMoSp*, 240, 127  
 Ilyushin, V., Alekseev, E., Dyubko, S., Motiyenko, R., & Lovas, F. 2005, *JMoSp*, 231, 15  
 Ioppolo, S., Fedoseev, G., Chuang, K. J., et al. 2021, *NatAs*, 5, 197  
 Jiménez-Serra, I., Bourke, T., Martín-Pintado, J., & Caselli, P. 2008, *A&A*, 482, 549  
 Jiménez-Serra, I., Martín-Pintado, J., Rivilla, V. M., et al. 2020, *AsBio*, 20, 1048  
 Jiménez-Serra, I., Rodríguez-Almeida, L. F., Martín-Pintado, J., et al. 2022, *A&A*, 663, A181  
 Jiménez-Serra, I., Vasyunin, A. I., Caselli, P., et al. 2016, *ApJL*, 830, L6  
 Jones, P. A., Cunningham, M. R., Godfrey, P. D., & Cragg, D. M. 2007, *MNRAS*, 374, 579  
 Kuan, Y.-J., Charnley, S. B., Huang, H.-C., Tseng, W.-L., & Kisiel, Z. 2003, *ApJ*, 593, 848  
 Lattalais, M., Puzat, F., Pilmé, J., Ellinger, Y., & Ceccarelli, C. 2011, *A&A*, 532, A39  
 Ligterink, N. F. W., Calcutt, H., Coutens, A., et al. 2018, *A&A*, 619, A28  
 Lovas, F. J., Kawashima, Y., Grabow, J. U., et al. 1995, *ApJL*, 455, L201  
 Maris, A. 2004, *PCCP*, 6, 2611  
 Marstokk, K., & Mollendal, H. 1999, *Acta Chem. Scand.*, 53, 79  
 Martín, S., Martín-Pintado, J., Blanco-Sánchez, C., et al. 2019, *A&A*, 631, A159  
 Martín, S., Requena-Torres, M. A., Martín-Pintado, J., & Mauersberger, R. 2008, *ApJ*, 678, 245  
 Martín-Pintado, J., Rizzo, J. R., de Vicente, P., Rodríguez-Fernández, N. J., & Fuente, A. 2001, *ApJL*, 548, L65  
 Marty, B., Altwegg, K., Balsiger, H., et al. 2017, *Sci*, 356, 1069  
 Megías, A., Jiménez-Serra, I., Martín-Pintado, J., et al. 2023, *MNRAS*, 519, 1601  
 Mininni, C., Beltrán, M. T., Rivilla, V. M., et al. 2020, *A&A*, 644, A84  
 Muñoz Caro, G. M., Meierhenrich, U. J., Schutte, W. A., et al. 2002, *Natur*, 416, 403  
 O'Brien, D. P., Izidoro, A., Jacobson, S. A., Raymond, S. N., & Rubie, D. C. 2018, *SSRv*, 214, 47  
 Oró, J. 1961, *Natur*, 190, 389  
 Padovani, M., Henebelle, P., & Galli, D. 2013, *A&A*, 560, A114  
 Pasek, M. A. 2008, *PNAS*, 105, 853  
 Pearce, B. K., Pudritz, R. E., Semenov, D. A., & Henning, T. K. 2017, *PNAS*, 114, 11327  
 Pickett, H. M., Poynter, R. L., Cohen, E. A., et al. 1998, *JQSRT*, 60, 883  
 Pizzarello, S., Cooper, G. W., & Flynn, G. J. 2006, in *The Nature and Distribution of the Organic Material in Carbonaceous Chondrites and Interplanetary Dust Particles (Space Science Series)* ed. D. S. Lauretta & H. Y. McSween (Tucson, AZ: Univ. of Arizona Press), 625  
 Potiszil, C., Ota, T., Yamanaka, M., et al. 2023, *NatCo*, 14, 1482  
 Requena-Torres, M. A., Martín-Pintado, J., Martín, S., & Morris, M. R. 2008, *ApJ*, 672, 352  
 Requena-Torres, M. A., Martín-Pintado, J., Rodríguez-Franco, A., et al. 2006, *A&A*, 455, 971  
 Rivilla, V. M., Beltrán, M. T., Martín-Pintado, J., et al. 2017, *A&A*, 599, A26  
 Rivilla, V. M., Colzi, L., Jiménez-Serra, I., et al. 2022a, *ApJL*, 929, L11  
 Rivilla, V. M., Drozdovskaya, M. N., Altwegg, K., et al. 2020a, *MNRAS*, 492, 1180  
 Rivilla, V. M., García De La Concepción, J., Jiménez-Serra, I., et al. 2022b, *FrASS*, 9, 829288  
 Rivilla, V. M., Jiménez-Serra, I., García de la Concepción, J., et al. 2021a, *MNRAS*, 506, L79  
 Rivilla, V. M., Jiménez-Serra, I., Martín-Pintado, J., et al. 2021b, *PNAS*, 118, 2101314118

- Rivilla, V. M., Jiménez-Serra, I., Martín-Pintado, J., et al. 2022c, *FrASS*, **9**, 876870
- Rivilla, V. M., Jiménez-Serra, I., Zeng, S., et al. 2018, *MNRAS*, **475**, L30
- Rivilla, V. M., Martín-Pintado, J., Jiménez-Serra, I., et al. 2019, *MNRAS*, **483**, L114
- Rivilla, V. M., Martín-Pintado, J., Jiménez-Serra, I., et al. 2020b, *ApJL*, **899**, L28
- Rodríguez-Almeida, L. F., Jiménez-Serra, I., Rivilla, V. M., et al. 2021a, *ApJL*, **912**, L11
- Rodríguez-Almeida, L. F., Rivilla, V. M., Jiménez-Serra, I., et al. 2021b, *A&A*, **654**, L1
- Rubin, M., Bekaert, D. V., Bradley, M. W., Drozdovskaya, M. N., & Wampfler, S. F. 2019, *ECS*, **3**, 1792
- San Andrés, D., Colzi, L., Rivilla, V. M., et al. 2023, *MNRAS*, **523**, 3239
- Sanz-Novo, M., Alonso, J. L., Rivilla, V. M., et al. 2022a, *A&A*, **666**, A134
- Sanz-Novo, M., Belloche, A., Alonso, J. L., et al. 2020, *A&A*, **639**, A135
- Sanz-Novo, M., Belloche, A., Rivilla, V. M., et al. 2022b, *A&A*, **666**, A114
- Sanz-Novo, M., Largo, A., Redondo, P., & Barrientos, C. 2019, *ECS*, **3**, 1170
- Sanz-Novo, M., Rivilla, V. M., Jiménez-Serra, I., et al. 2023, arXiv:2307.08644
- Sánchez-Monge, Á., Schilke, P., Schmiedeke, A., et al. 2017, *A&A*, **604**, A6
- Shingledecker, C. N., Álvarez-Barcia, S., Korn, V. H., & Kästner, J. 2019, *ApJ*, **878**, 80
- Snyder, L. E., Lovas, F. J., Hollis, J. M., et al. 2005, *ApJ*, **619**, 914
- Tercero, B., Kleiner, I., Cernicharo, J., et al. 2013, *ApJL*, **770**, L13
- Tercero, F., López-Pérez, J. A., Gallego, J. D., et al. 2021, *A&A*, **645**, A37
- Yusef-Zadeh, F., Cotton, W., Wardle, M., & Intema, H. 2016, *ApJL*, **819**, L35
- Yusef-Zadeh, F., Muno, M., Wardle, M., & Lis, D. C. 2007, *ApJ*, **656**, 847
- Zeng, S., Jiménez-Serra, I., Rivilla, V. M., et al. 2018, *MNRAS*, **478**, 2962
- Zeng, S., Jiménez-Serra, I., Rivilla, V. M., et al. 2021, *ApJL*, **920**, L27
- Zeng, S., Rivilla, V. M., Jiménez-Serra, I., et al. 2023, *MNRAS*, **523**, 1448
- Zeng, S., Zhang, Q., Jiménez-Serra, I., et al. 2020, *MNRAS*, **497**, 4896